

Liquid Nitrogen Passivation for Deep-Blue Perovskite Quantum Dots with Nearly Unit Quantum Yield

Xiaodong Peng,[†] Cheng Yan,[†] Fengjun Chun,[†] Wen Li, Xiankan Zeng, Xuehai Fu, Yue Gao, Xiang Chu, Guo Tian, and Weiqing Yang*



Cite This: *J. Phys. Chem. C* 2022, 126, 1017–1025



Read Online

ACCESS |



Metrics & More



Article Recommendations



Supporting Information

ABSTRACT: Deep-blue metal halide perovskite light-emitting diodes (PeLEDs) (450–470 nm) still fall behind their green and red counterparts in terms of efficiency, luminance, and lifetime, badly suffering from excess intrinsic surface defects of metal halide perovskites. Herein, we presented a liquid nitrogen passivation (LNP) strategy to effectively restrain the defects of surface Br vacancy (V_{Br}) for high-quality deep-blue MAPbBr₃ quantum dots (QDs). This liquid nitrogen (LN) provides a low-temperature environment to reduce the size of MAPbBr₃ QDs for the green-to-deep-blue emission transformation and impel NH₄Br to firmly anchor surface Br ions for V_{Br} passivation. These irreversible deep-blue MAPbBr₃ QDs remarkably feature the high photoluminescence quantum yield of 97.64% and the strong stability of 91% remaining photoluminescence intensity against ultraviolet irradiation after 120 min, which are comparable to those of red/green counterparts. Based on these findings, we developed deep-blue PeLEDs with the electroluminescence emission of 455 nm, which is in line with the standard of the National Television Standards Committee (NTSC). Evidently, this LNP strategy may open a way to transform the emission spectra and achieve high-quality deep-blue perovskite QDs, promoting the commercial development of deep-blue PeLEDs.



INTRODUCTION

Metal halide perovskite light-emitting diodes (PeLEDs) have shown great potential as emerging emitters for the next-generation solid-state lighting due to narrow full width at half-maximum (FWHM), wide color gamut, and low-cost solution process.^{1–7} Currently, the advanced PeLEDs regarding green/red PeLEDs have been made impulsive progress with high external quantum efficiencies boosted to 23.4%⁸ and 23%,⁹ respectively. However, the performance of deep-blue PeLEDs (450–470 nm), which is imperative for NTSC requirements of next-generation displays, still lag behind their green and red counterparts.^{7,10,11} This backwardness is simultaneously ascribed to the thorny preparation and excess intrinsic surface defects of deep-blue perovskites.^{11–13}

Generally, the synthesis methods of deep-blue perovskites can be classified into two categories: compositional regulation¹⁴ and dimensional engineering.¹⁵ On one hand, compositional regulation employs mixed (Cl/Br) halide perovskites to widen the band gap in the blue-region spectra.¹⁶ Although mixed Br/Cl can readily achieve deep-blue spectra, phase segregation of mixed halide perovskites under external field is unfavorable for spectrally stable PeLEDs.¹⁷ On the other hand, dimensional engineering expands the band gap under the strong quantum confinement effect for deep-blue emission by reducing some spatial dimension of pure-bromide perovskites.¹⁸ However, there are a large number of Br vacancy (V_{Br}) defects on the crystal surface due to the high surface-to-volume ratio, which seriously aggravates the optical properties of small-sized deep-blue QDs.^{19,20} The acid-etching-driven ligand-exchange strategy

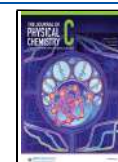
was promoted to obtain deep-blue (470 nm) CsPbBr₃ QDs.¹¹ Nevertheless, this strategy, which uses the hot-injection method, is not suitable for practical application owing to its complexity and relatively high cost.

Furthermore, the V_{Br} defect formation in deep-blue QDs occurs due to various reasons. First, owing to the low defect formation energy at room temperature, the vacancy defects can be facily generated on the surface of perovskite QDs during the fast nucleation and growth process.^{21,22} Second, highly dynamic organic capping ligands, such as oleic acid (OA) and *n*-octylamine (OTAm), cannot stabilize the perovskite QD structure well, easily regenerating V_{Br} defects at room temperature.^{23–25} The inorganic ligands, such as PrCl₃,¹⁶ ZnBr₂,²⁶ and NaBr,¹⁵ can adhere to the QDs, forming a Br[−]-sufficient surface to inhabit the V_{Br} regeneration. To reduce the defect number within deep-blue perovskite QDs, their defects must be intensely suppressed during the synthesis process. Furthermore, vacancy defect renewal produced by excessive dynamic surface organic ligands should be occupied by selecting suitable inorganic ligands. As a result, it is crucial for developing a novel strategy for the simple fabrication of deep-blue perovskite QDs as well as the

Received: October 6, 2021

Revised: December 24, 2021

Published: January 5, 2022



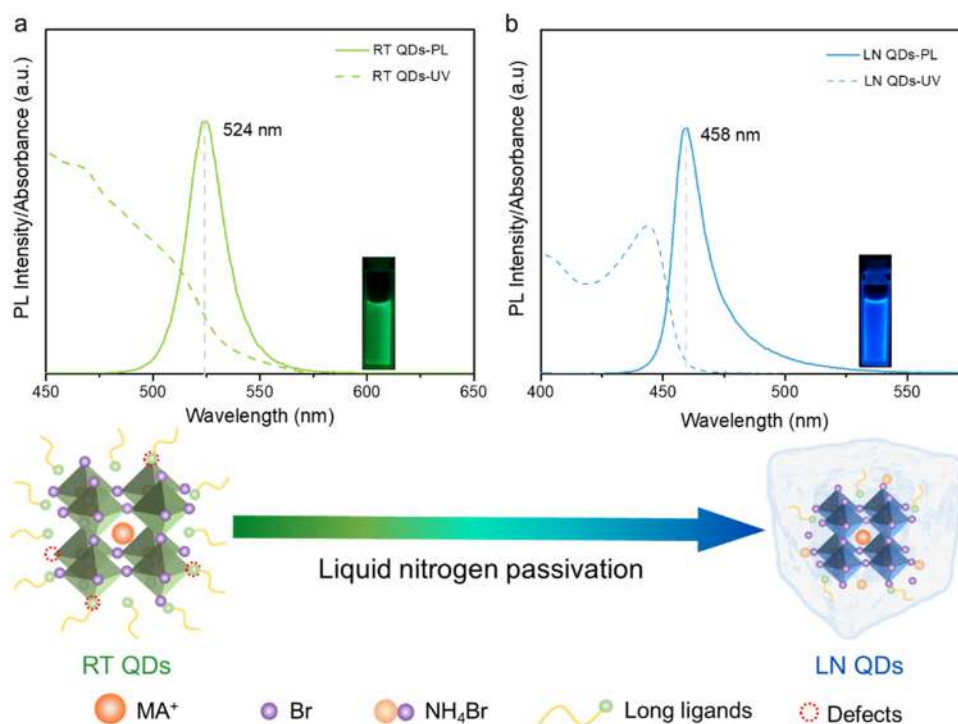


Figure 1. Photoluminescence spectra transformation of MAPbBr₃ QDs after liquid nitrogen passivation (LNP). (a) PL and absorption spectra of room-temperature (RT) QDs. (b) PL and absorption spectra of liquid nitrogen (LN) QDs. The insets show the photographs of RT and LN QDs under UV irradiation (365 nm). The bottom schematic diagram shows that the MAPbBr₃ QDs present deep-blue emission with low-density defects and fewer organic ligands after LNP.

effective passivation of V_{Br} exposed on the QD surface at the same time.

Herein, we design a liquid nitrogen passivation (LNP) strategy to transform the PL spectrum of MAPbBr₃ QDs from green emission to deep-blue emission and to restrain undesirable V_{Br} defects by NH₄Br for the enhancement of PLQY simultaneously. As for MAPbBr₃ QDs, the LN can play a critical role in nucleation, growth, and surface V_{Br} defect passivation. Owing to the suppression of nucleate and growth rates at extremely low temperatures, MAPbBr₃ QDs present a strongly confined size of 2.12 nm and an intense deep-blue emission of 458 nm. Moreover, benefiting from the high defect formation energy at cryogenic temperature, the introduced NH₄Br can firmly anchor surface Br⁻ ions for the passivation of V_{Br} defects and reconstruct the surface–ligand environment for the regeneration of V_{Br} defects. Based on the LNP strategy, the optimized MAPbBr₃ QDs facilitate achieve a near-unity PLQY of 97.64%. In addition, the MAPbBr₃ QD film demonstrates the remarkable UV irradiation stability of 91% remaining photoluminescence intensity after 120 min. Further, we successfully fabricated the deep-blue PeLEDs with electroluminescence (EL) emission of 455 nm, which is consistent with the deep-blue standard of NTSC. This strategy may open a way to transform the emission spectra and achieve high-quality deep-blue perovskite QDs, promoting the commercial development of deep-blue PeLEDs.

METHODS

Deep-blue MAPbBr₃ QDs with liquid nitrogen passivation (LNP QDs) were synthesized using a modified ligand-assisted reprecipitation (LARP) method at low temperatures (190 K). MABr (0.1 mmol), 0.1 mmol NH₄Br, and 0.12 mmol PbBr₂ were dissolved in 3 mL of DMF. A certain amount of liquid

nitrogen was put into 10 mL of toluene containing 5 μL of *n*-octylamine and 200 μL of oleic acid. After about 20 s, when “bad solvent” toluene is cooled to 190 K, measured by a low-temperature thermometer, 200 μL of the precursor solution was quickly injected into toluene. After about 15 min, a strong blue PL emission was observed under ultraviolet lamp excitation. After centrifuging at 8000 rpm for 8 min using a refrigerated centrifuge to discard the unreacted precipitate, a bright supernatant blue solution was obtained. Green MAPbBr₃ QDs (RT QDs) were obtained by the traditional LARP at room temperature (298.15 K). Briefly, 200 μL of a precursor containing 0.1 mmol MABr and 0.12 mmol PbBr₂ was injected into 10 mL of the toluene solution with similar organic ligand contents. Details of the material information and device fabrication can be found in the [Supporting Information](#).

RESULTS AND DISCUSSION

Colloidal MAPbBr₃ QDs synthesized by the traditional LARP method at room temperature only emit a 524 nm green emission spectrum (Figure 1a).^{27,28} Nevertheless, employing a feasible LNP strategy, the significantly blue-shifted MAPbBr₃ QDs were successfully prepared. In brief, we lowered the reaction temperature to 190 K using liquid nitrogen and subsequently injected pre-prepared precursor solution containing MABr, PbBr₂, and NH₄Br into the cryogenic toluene solution (see detailed information in [Figure S1](#), [Methods](#), and [Video S1](#)). Consequently, the MAPbBr₃ QDs treated by LN (LN QDs) exhibited a sharp deep-blue PL emission at 458 nm and an obvious exciton absorption at 443 nm (Figure 1b). These deep-blue LN QDs had a narrower FWHM of 15 nm, indicating high deep-blue color purity. From the results of respective absorption Tauc plots, the band gap of MAPbBr₃ QDs extends from 2.30 to 2.70 eV after the introduction of LN (Figure S2 and eq 1 in the

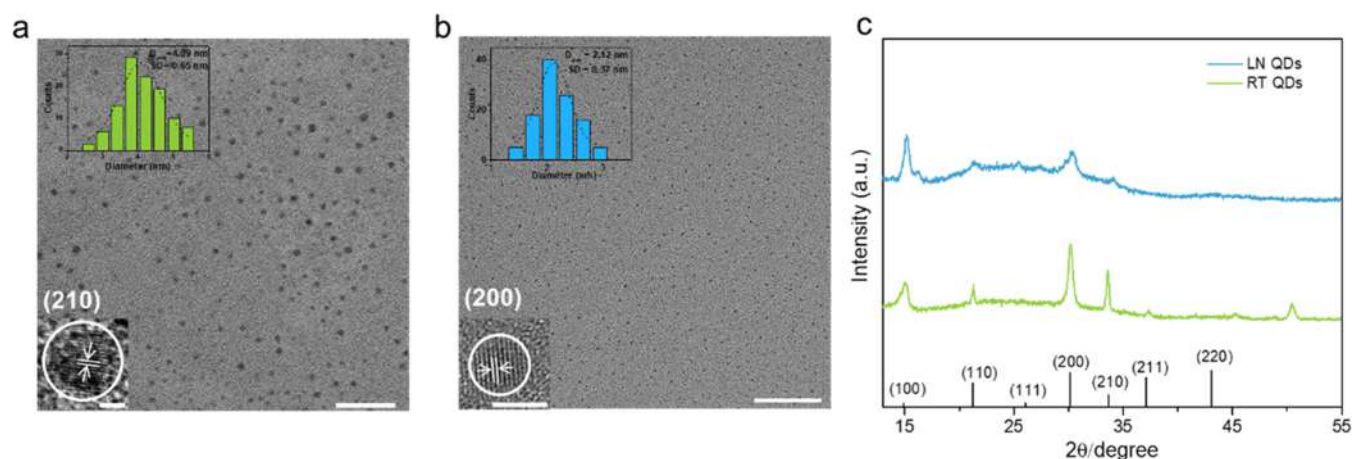


Figure 2. Morphology and optical properties of MAPbBr₃ QDs. Transmission electron microscopy (TEM) images of (a) RT QDs and (b) LN QDs. The scale bar is 50 nm. The inset at the bottom of the image represents the respective high-resolution TEM. The scale bar is 2 nm. The inset at the top of the image shows the corresponding particle size distribution of QDs. (c) XRD patterns of RT and LN QDs.

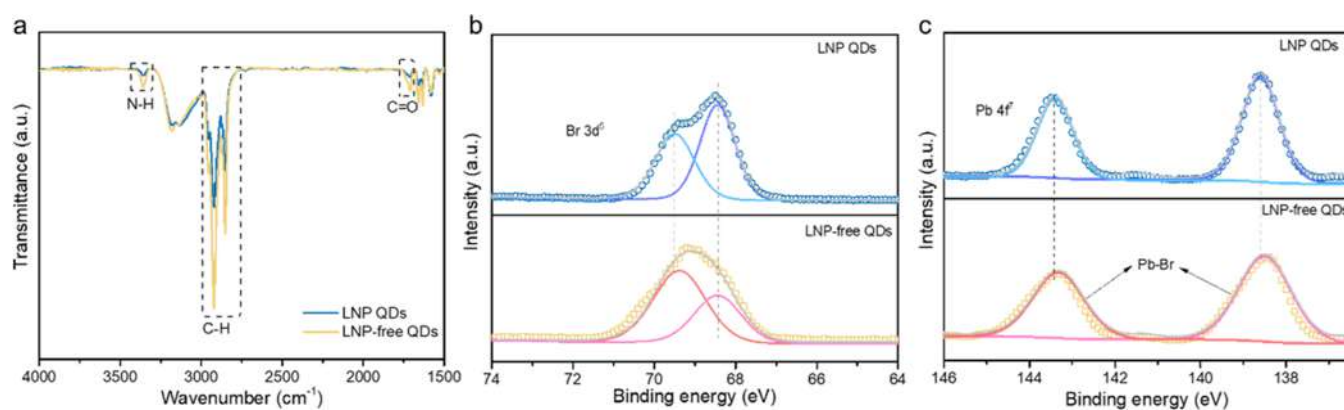


Figure 3. Surface states of LNP QDs and LNP-free QDs. (a) FTIR results. (b) High-resolution Br 3d XPS spectra of QDs. (c) High-resolution XPS spectra for Pb 4f.

Supporting Information). Compared with RT QDs, the LN QDs with the strong quantum confinement effect show a remarkable blue-shift in PL emission (66 nm), which proves that the deep-blue QDs could be easily obtained by the LN treatment.

To investigate the nanostructure of RT QDs and LN QDs, transmission electron microscopy (TEM) and high-resolution TEM (HRTEM) were utilized. The RT QDs presented an average particle size of 4.09 nm with a size deviation of ± 0.65 nm (Figure 2a). The related crystal structure was further revealed by HRTEM (the inset). According to HRTEM, the interplanar distances of RT QDs is 2.63 Å, matching along with the (210) crystal plane.²⁹ Notably, under different experimental conditions, the sizes of green-emitting RT QDs are different.³⁰ Figure 2b demonstrates the nanostructure details of the LN QDs. It has been reported that MAPbBr₃ QDs with a size close to 2 nm possess an intensive quantum confinement effect.³¹ The average particle size of LN QDs was 2.12 ± 0.37 nm with an interplanar distance of 2.97 Å, corresponding to the (200) crystal plane of the cubic MAPbBr₃.³¹ The results of the XRD diffraction peak are consistent with those of the respective TEM and HRTEM (Figure 2c). The XRD pattern for RT QDs exhibited main peaks at 15.0, 21.3, 30.2, and 33.7°, corresponding to the (100), (110), (200), and (210), respectively. However, for LN QDs, there were primary peaks with border half peak width at 15.1, 21.3, 30.3, and 33.8°, which

indicated that LN QDs have smaller particle sizes than those of RT QDs according to the Scherrer equation.³² Generally, the smaller the nanoparticle size, the stronger the quantum confinement effect, which contributes to the blue-shift in luminescence.¹⁸ The size of LN QDs was smaller than that of RT QDs, indicating that the LN passivation strategy can remarkably reduce the QD size for enlarging the band gap of QDs.

The lower the reaction ambient temperature, the higher the defect formation energy, which indicates fewer defects in pristine deep-blue QDs.^{33–35} However, long-time exposure to air causes the generation of defects again in pristine QDs owing to the active ion migration.³⁶ Also, ultrasmall deep-blue QDs would grow slowly, leading to poor size uniformity due to excessive dynamic organic ligands.¹⁶ Replacing the traditional long alkyl ligands by inorganic ligands has been put forward to improve their optical performances and stabilize perovskite QDs.^{9,37} Hence, we introduced NH₄Br salts in an LN-aided process to repair undesirable V_{Br} defects and reconstruct surface–ligand environment for firmly fixing deep-blue properties of QDs. Briefly, by the usage of LN, NH₄Br-treated and NH₄Br-free QDs were, respectively, denoted as LNP QDs and LNP-free QDs. To demonstrate this strategy, the LNP/LNP-free QDs were dissected to explore the surface capping ligands and defects. Figure 3a illustrates the results of the Fourier transform infrared spectrum (FTIR). The obviously decreased peak intensity in the range 2700–3000 cm⁻¹ (attributed to the

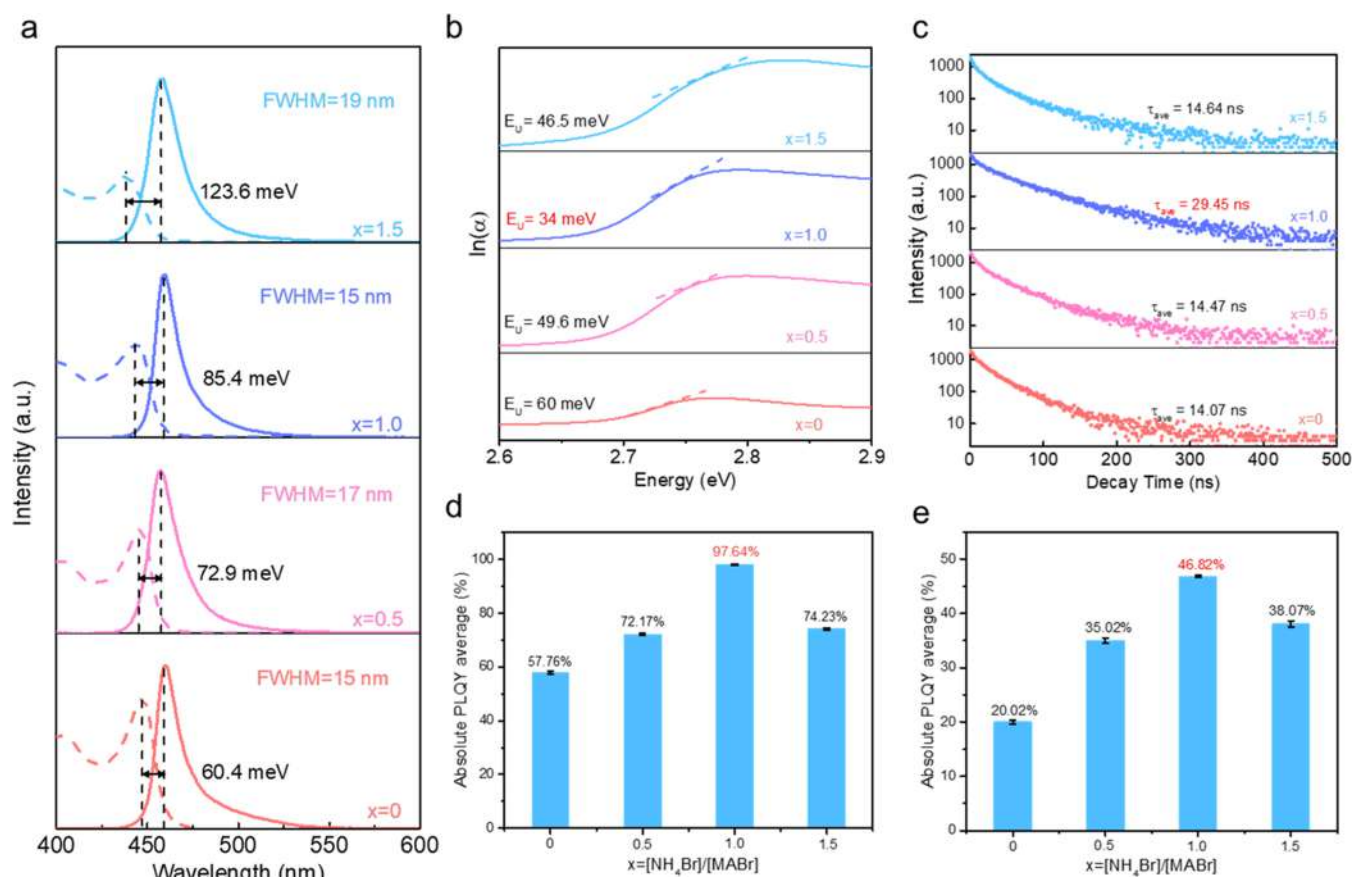


Figure 4. Evolution of the emissive performance with different x values (x is defined as the ratios of NH_4Br and MABr , $x = 0, 0.5, 1.0, 1.5$). (a) PL and absorption spectra of the corresponding samples. (b) TRPL spectra. (c) Absorption curves for the calculation of Urbach energy (E_U). (d) Absolute PLQY value of QD colloidal solution and (e) related spin-coated films on ITO/PEDOT:PSS/PVK substrates for a series of x values.

saturated vibration of C–H) indicated that organic ligands were partially replaced by NH_4Br after LNP. In addition, the C=O stretching vibration of the carboxylate group at 1712 cm^{-1} was weakened after LNP, confirming the notable decrease in OA.³² The stretching vibration peak of the $-\text{NH}_2$ group existing in OTAm is located at 3358 cm^{-1} , the characteristic signal of which is weakened as well. Furthermore, XPS characterization was utilized to further analyze the surface defect states of LNP and LNP-free QDs. As illustrated in Figure 3b, the Br 3d spectrum can be separated into two peaks, corresponding to the higher binding energy peak of surface Br^- ions and the lower binding energy peak of inner Br^- ions.^{27,28} The surface Br^- peak (69.49 eV) of LNP QDs shifted to higher binding energies compared with LNP-free QDs, suggesting the sufficient passivation of surface V_{Br} and the strong Pb–Br interaction by LNP strategy.^{28,38,39} In addition, the level of Br in the LNP QDs increased because of the enhancement of the Br/Pb ratio (Figure S3), implying that V_{Br} was notably decreased. Compared with the LNP-free QDs, the Pb $4f_{5/2}$ (143.40 eV) and $4f_{7/2}$ (138.62 eV) peaks in the Pb 4f spectra for LNP QDs shifted toward higher binding energy of 0.12 eV, indicating a stronger Pb–Br bond and improved chemical environment of octahedral $[\text{PbBr}_6]^{4-}$ in LNP QDs (Figure 3c).³⁹ In Figure S3, the high-resolution XPS spectrum of N 1s for the LNP-free QDs can be fitted into two peaks at 401.8 eV and 399.9 eV, which correspond to the protonated groups ($-\text{NH}_3^+$) and the amine groups ($-\text{NH}_2$), respectively.²⁵ However, for LNP QDs, the N 1s core level can be deconvoluted in other two peaks: the

$-\text{NH}_3^+$ peak at 401.8 eV and the NH_4^+ peak at 402.2 eV. The disappearance of the peak at 399.9 eV for the amine group and the appearance of the peak at 402.2 eV for NH_4^+ shown in Figure S3 demonstrated that excess surface organic ligands were replaced by NH_4Br . Also, the oxygen content in the O/Pb atom ratio of XPS reduced remarkably from 2.15 (LN-free QDs) to 1.35 (LN QDs) in Figure S3. This result also demonstrated that some organic OA ligands were substituted by NH_4Br because O atoms are present only in OA. Combined with FTIR and XPS results, this result confirms the validity mechanism of the LNP strategy, in which NH_4Br can bond with Br^- ions as inorganic ligands for a decrease in the long-chain organic ligands and adhered it to the surface of QDs for promoting the formation of Br^- -rich surface with the decrease of V_{Br} . Consequently, the spin-coated perovskite films showed different morphologies, as revealed by atomic force microscopy (AFM) diagrams in Figure S4. The LNP-free QD films showed a large root-mean-square (RMS) roughness of 5.76 nm, resulting from the plentiful organic ligands.³² Also, LNP QD films with less capping organic ligands presented a decreased RMS of 4.63 nm. Herein, NH_4Br , as an inorganic ligand, plays the role of surface defect passivation without affecting the perovskite crystal structure. To verify this, we carried out XRD and TEM characterization. Figure S5 demonstrates that the LNP-free QDs presented an average particle size of 2.22 nm, which is similar to the size of LNP QDs. Also, the radius of NH_4^+ (1.46 Å) is much smaller than that of MA^+ (2.17 Å), which leads to the limited ability to shape a stable perovskite structure.⁴⁰ Compared with LNP-free QDs, no

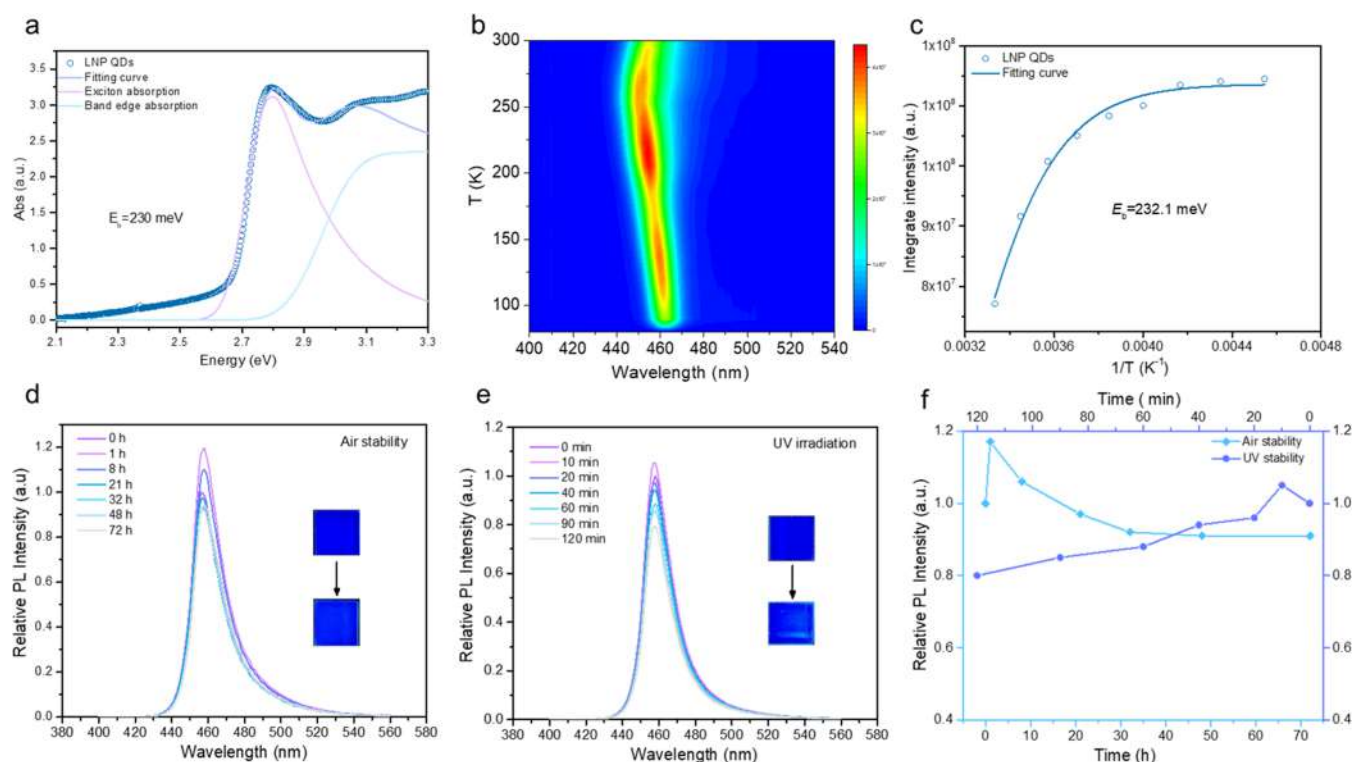


Figure 5. Exciton dynamic characterization and stability test. (a) Measured Abs spectrum with fitting curves. (b) Measured temperature-dependent PL spectra curves for E_U calculation of LNP QDs. (c) Integrated PL intensity as a function of the reciprocal of temperature. (d) Air stability test of the film of LNP QDs (T : 298.35 K; RH: 54.3%). (e) UV stability test of the film of LNP QDs (365 nm, 20 W). (f) Normalized PL intensity as a function of time for LNP QDs.

diffraction peak shift appeared in the LNP QDs ($x = 0.5, 1.0, 1.5$) in Figure S5, proving that NH_4^+ is anchored on the surface of QDs rather than being incorporated into the QD crystal lattice.

To explore the optimum content of NH_4Br , MAPbBr_3 QDs were synthesized with the addition of a series of concentrations of NH_4Br salts. Also, x was defined as the molar ratio of ammonium bromide to methylamine bromide ($x = \text{NH}_4\text{Br}/\text{MABr}$), including $x = 0, 0.5, 1$, and 1.5 . As shown in Figure 4a, all four samples exhibited similar emission peaks at 458 nm, while their first exciton absorption peaks are located at 447 nm ($x = 0$), 445 nm ($x = 0.5$), 443 nm ($x = 1.0$), and 437 nm ($x = 1.5$). The LNP QDs ($x = 0.5, 1.0, 1.5$) have a larger Stokes shift than the LNP-free QDs ($x = 0$) according to the results in Figure S6. As the content of NH_4Br increased to $x = 1.5$, the LNP QDs showed the largest Stokes shift (123.6 meV) and the widest FWHM (19 nm). Compared with the TEM diagrams of each sample in Figure S5, the $x = 1.5$ LNP QDs have a wider size distribution leading to the above results.⁴¹ This larger Stokes shift in perovskite QDs results in lower self-absorption, which is good for the improvement in PLQY of the perovskite film.⁴² Additionally, the relative optical band gap is almost unchanged with the addition of different concentrations of NH_4Br , displaying a wide band gap value (~ 2.70 eV) calculated from eq 1 in the Supporting Information and Figure S7. The degree of crystal disorder of MAPbBr_3 QDs as direct band gap semiconductors is related to the absorption edge (Urbach tail). To evaluate the V_{Br} defect density in deep-blue MAPbBr_3 QDs, Urbach energies (E_U) of the samples were calculated by the absorption coefficient as a function of photon energy (eq 2 in the Supporting Information). Generally, a smaller E_U value indicates the fewer defects in perovskites.⁴³ As depicted in

Figure 4b, the E_U of the LNP-free QDs is 60 meV, while those of the LNP QDs are obviously reduced to 34 meV ($x = 1$), 46.5 meV ($x = 1.5$), and 49.6 meV ($x = 0.5$), indicating that the defect states have been significantly passivated in LNP QDs. Moreover, the TRPL was utilized to analyze the exciton recombination dynamics for LNP-free QDs and LNP QDs in Figure 4c. Time-resolved PL decay (TRPL) was carried out to demonstrate the LNP advantages in decay kinetics. Also, average lifetimes (τ_{ave}) can be calculated by eqs 3 and 4 in the Supporting Information. Obviously, LNP QDs presented a longer average lifetime (29.45 ns) than the LNP-free QDs (14.07 ns), demonstrating that nonradiative recombination originating from defect-related fast exciton trapping was effectively eliminated,³ especially for the samples of $x = 1$ (Table S1). Furthermore, we tested the PLQY of colloidal QD solutions and spin-coated films with different concentrations of NH_4Br (Figures 4d,e, S8, and S9). The PLQY of the deep-blue QDs regarding the colloidal solution with different NH_4Br contents ($x = 0, 0.5, 1$) notably increased from 57.64 to 97.64%. As the contents further increase ($x = 1.5$), the PLQY slightly dropped to 74.23%, which might be attributed to excessive NH_4^+ . Excess NH_4^+ cations will affect the periodicity of the perovskite host lattice, hindering the charge transport and weakening the luminescence properties of host perovskites.⁴⁴ Certainly, the PLQY of the related spin-coated films for the deep-blue QDs also showed the same trend with a colloidal solution. Among these remaining samples, the $x = 1$ sample film showed the highest value of PLQY (46.82%). These results revealed that the LNP QDs with the best NH_4Br addition amount ($x = 1$) have the lowest defect density (E_U : 34 meV) and the highest PLQY (97.64%).

To probe into the carrier dynamics of LNP QDs more deeply, the logarithmic absorption and time-temperature PL spectra

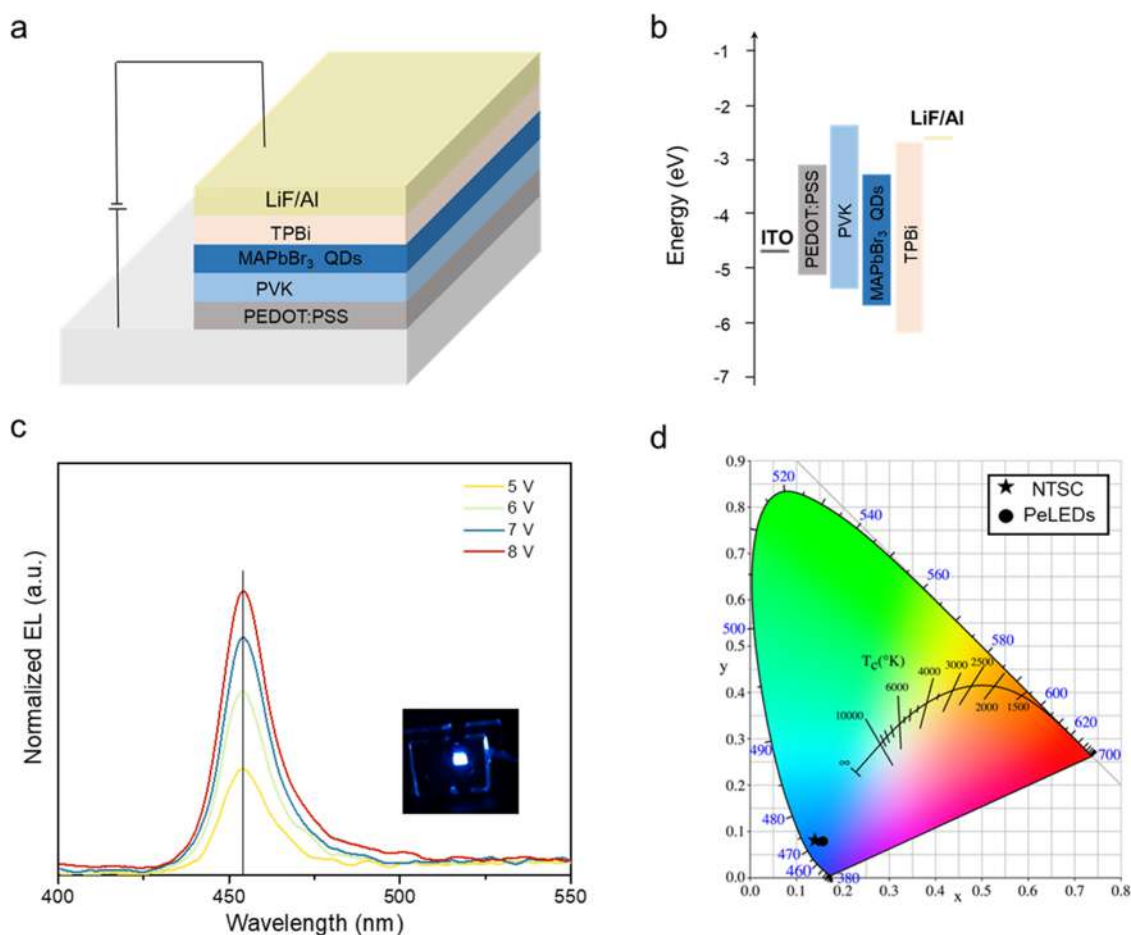


Figure 6. Deep-blue LED based on NNP QDs. (a) Device architecture. (b) Energy-level diagram. (c) CIE coordinates of the deep-blue LED. (d) Electroluminescence spectra of the deep-blue LEDs at different driven voltages.

were utilized. Ultrasmall deep-blue QDs with a strong confinement effect could result in a high exciton binding energy (E_b). More importantly, the stronger the binding energy, the more efficient the exciton recombination.¹² Exciton binding energy can be extracted from logarithmic absorption spectra using eqs 5 and 6

$$p(E) = p_x + \frac{A_c}{2} \left[\operatorname{erf} \left(\frac{(E - E_0) - E_b^x}{\gamma_c} \right) + 1 \right] \quad (5)$$

$$p_x = \frac{1}{2\eta} \left[\operatorname{erf} \left(\frac{E - E_0}{\gamma} - \frac{\gamma}{2\eta} \right) + 1 \right] \exp \left(\frac{\gamma^2}{4\eta^2} - \frac{E - E_0}{\eta} \right) \quad (6)$$

where p_x is the absorption curve with asymmetric broadening η . γ , γ_c and A_c are the line width of the absorption peak, width of continuous edge, and step height, respectively.⁴⁵ E_0 and E_b^x are the absolute exciton energy and the binding exciton energy, respectively. There is an obvious exciton absorption peak in the logarithm-treatment absorption line, indicating that E_b can be acquired from the band edge absorption fitting. As illustrated in Figures 5a and S10, the E_b of LNP QDs (230 meV) is larger than that of LNP-free QDs (187 meV), which means that more effective exciton radiative recombinations are formed in LNP QDs. Also, E_b can be obtained from the temperature-dependent PL spectra to confirm the veracity of the above result E_b from the absorption spectra. E_b can be calculated using eq 7

$$I(T) = \frac{I_0}{1 + A e^{-E_b/k_B T}} \quad (7)$$

where I_0 is the maximum integrated intensity, E_b is the exciton binding energy, and k_B is the Boltzmann constant.^{46,47} The fitted E_b of LNP QDs is 232.1 meV from the temperature-dependent PL spectra in Figure 5b,c. However, the LNP-free QDs possessed a smaller value of E_b (188.6 meV) in Figure S11 than that of LNP QDs, which is consistent with the logarithmic absorption spectra results. In comparison with LNP-free QDs, there are more effective radiative recombinations in LNP QDs from the fitted results of E_b , demonstrating the superiority of LNP for deep-blue QDs. Moreover, the stability of deep-blue LNP QDs against the pernicious effect of air and UV-light irradiation was tested. Although the stability of perovskite QDs was assessed in terms of colloidal solutions from different reported works, the QDs were protected by nonpolar solvents (e.g., toluene, hexane). The stability of colloidal QD solution has little significance for commercialized deep-blue perovskite LEDs.⁴⁸ Therefore, the film stability, comprising air stability and photostability, is more direct and pivotal compared with that of colloidal solutions for deep-blue light-emitting diodes in the future. As depicted in Figure 5d, the film of LNP QDs maintained 91% initial intensity after 72 h under the environmental conditions (T : 298.35 K; RH: 54.3%). We also investigated the stability without any encapsulation under continuous ultraviolet irradiation. The film can retain 80% intensity after 120 min under intense irradiation (Figure 5e). In

addition, Figure 5f evidently presents the strong air stability and photostability for LNP QDs. However, for LNP-free QDs, the spin-coated film exhibited lower air stability (40% of initial PL intensity) after 72 h and irradiation stability (46% of initial PL intensity) after 120 min UV irradiation than LNP QD film (Figure S12).

Subsequently, we fabricated deep-blue PeLEDs by applying a typical multilayered structure of ITO/PEDOT:PSS/PVK/MAPbBr₃ QDs/TPBi/LiF/Al (Figure 6a). Notably, both the hole transport layer (HTL) and perovskite layer were prepared by a solution-based spin-coating method with a period of annealing treatment. Also, the higher layers, comprising TPBi (30 nm), LiF (10 nm), and Al electrodes (100 nm), were deposited by vacuum evaporation equipment. Figure 6b depicts the schematic band structure of deep-blue LEDs. As shown in Figure 6c, deep-blue PeLEDs based on LNP QDs exhibited an EL emission peak at 455 nm, with high color purity (FWHM, 19.4 nm). The deep-blue EL emission of the related devices adhered to the Commission International de l'Eclairage coordinates (0.17, 0.07), stratifying the required blue gamut in the range of CIE (γ coordinates <0.1),⁴⁹ as revealed in Figure 6d. Other performance data of the deep-blue perovskite LED, including current density, luminance, and external quantum efficiency, are shown in Figure S13.

The excellent deep-blue LNP QDs with good color purity, high PLQY, and strong stability should be mainly attributed to the following factors. For starters, liquid nitrogen, an inert and freezing liquid, can swiftly lower the reaction temperature without affecting the crystal structure or ligands. Second, the cryogenic liquid nitrogen environment strongly confines the size of MAPbBr₃ QDs, resulting in a significant shift from green to deep-blue emission. Under the strong quantum confinement effect, liquid nitrogen provides low-temperature reaction conditions that suppress the nucleation and growth of MAPbBr₃ QDs, causing the QD size to decrease dramatically and the band gap to enlarge noticeably. Third, the high defect formation energy in a low-temperature atmosphere is favorable for reducing defect generation during the synthesis process. The thermal defect concentration in ionic crystals is affected by temperature. In general, the low synthesis temperature restricts the thermal movement of ions, resulting in less vacancy defect formation. Fourth, the abundant NH₄Br in the LNP process can not only passivate the V_{Br} defects but also reconstruct the surface–ligand environment of QDs, hence fixing their excellent deep-blue optical properties.

Consequently, this work proved the large potential of LNP for the easy preparation of high-performance deep-blue perovskite QDs, underpinning the development of deep-blue PeLEDs.

CONCLUSIONS

In summary, we report a novel strategy of liquid nitrogen passivation for producing high-quality deep-blue MAPbBr₃ QDs in a low-temperature environment. The strongly confined MAPbBr₃ QDs with an ultrasmall size of 2.12 nm present an intense deep-blue emission of 458 nm after the LNP strategy. To firmly fix the superior deep-blue optical properties, the introduced NH₄Br can anchor surface Br⁻ ions for the passivation of V_{Br} defects and reconstruct a surface–ligand environment for the inhabitation of V_{Br}. As a result, the LNP-treated deep-blue MAPbBr₃ QDs exhibit a high PLQY of up to 97.64%, originating from low-density defects (E_v: 34 meV), more radiative recombination ($\tau_{\text{ave}} = 29.45$ ns), and large exciton binding energy (230 meV). In addition, without any packaging

protection, the associated deep-blue films have resistant air stability of 70 h and UV stability of 120 min. Finally, the fabricated deep-blue PeLEDs based on LNP QDs show an EL emission at 455 nm, indicating some potential for commercialized blue lighting. As a result, our work contributes to the development of deep-blue PeLEDs by introducing a novel method for the easy preparation of superior deep-blue emission QDs.

ASSOCIATED CONTENT

Supporting Information

The Supporting Information is available free of charge at <https://pubs.acs.org/doi/10.1021/acs.jpcc.1c08765>.

Experimental details, additional characterization, calculation equations, and TRPL fitting parameters of LNP QDs and LNP-free QDs (Table S1), synthesis schematics (Figure S1), band gap calculations of RT QDs and LN QDs (Figure S2), XPS diagram (Figure S3), AFM morphology images (Figure S4), TEM and XRD (Figure S5), Stokes shift (Figure S6), band gap (Figure S7), measured absolute PLQY value (Figure S8), measured absolute PLQY results of related QD films (Figure S9), temperature-dependent PL spectra (Figure S11) of LNP QDs and LNP-free QDs, E_b calculation (Figure S10), stability test for related films (Figure S12) of LNP-free QDs, and other performance data of the deep-blue perovskite LED (Figure S13) (PDF)

Process of liquid nitrogen passivation strategy (Video S1) (MP4)

AUTHOR INFORMATION

Corresponding Author

Weiqing Yang – Key Laboratory of Advanced Technologies of Materials (Ministry of Education), School of Materials Science and Engineering, Southwest Jiaotong University, Chengdu 610031, China; orcid.org/0000-0001-8828-9862; Email: wqyang@swjtu.edu.cn

Authors

Xiaodong Peng – Key Laboratory of Advanced Technologies of Materials (Ministry of Education), School of Materials Science and Engineering, Southwest Jiaotong University, Chengdu 610031, China

Cheng Yan – Key Laboratory of Advanced Technologies of Materials (Ministry of Education), School of Materials Science and Engineering, Southwest Jiaotong University, Chengdu 610031, China

Fengjun Chun – Key Laboratory of Advanced Technologies of Materials (Ministry of Education), School of Materials Science and Engineering, Southwest Jiaotong University, Chengdu 610031, China

Wen Li – Key Laboratory of Advanced Technologies of Materials (Ministry of Education), School of Materials Science and Engineering, Southwest Jiaotong University, Chengdu 610031, China

Xiankan Zeng – Key Laboratory of Advanced Technologies of Materials (Ministry of Education), School of Materials Science and Engineering, Southwest Jiaotong University, Chengdu 610031, China

Xuehai Fu – Key Laboratory of Advanced Technologies of Materials (Ministry of Education), School of Materials Science

and Engineering, Southwest Jiaotong University, Chengdu 610031, China

Yue Gao – Key Laboratory of Advanced Technologies of Materials (Ministry of Education), School of Materials Science and Engineering, Southwest Jiaotong University, Chengdu 610031, China

Xiang Chu – Key Laboratory of Advanced Technologies of Materials (Ministry of Education), School of Materials Science and Engineering, Southwest Jiaotong University, Chengdu 610031, China

Guo Tian – Key Laboratory of Advanced Technologies of Materials (Ministry of Education), School of Materials Science and Engineering, Southwest Jiaotong University, Chengdu 610031, China

Complete contact information is available at:
<https://pubs.acs.org/10.1021/acs.jpcc.1c08765>

Author Contributions

[†]X.P., C.Y., and F.C. contributed equally to this work. W.Y. supervised the project. All of the authors participated in this work and discussed the results.

Notes

The authors declare no competing financial interest.

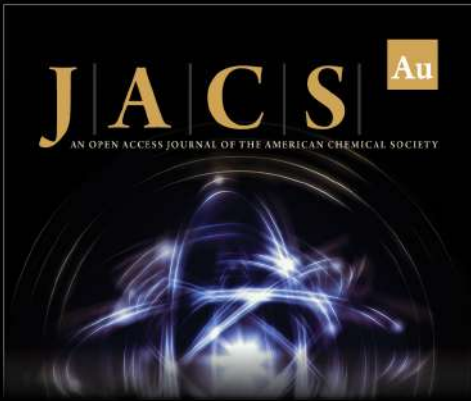
ACKNOWLEDGMENTS

This work was financially supported by Young Scientific and Technological Innovation Research Team Funds of Sichuan Province (Nos. 20CXTD0106 and 2019YFG0292) and Fundamental Research Funds for the Central Universities (No. 2682020CX06).

REFERENCES

- (1) Akkerman, Q. A.; Raino, G.; Kovalenko, M. V.; Manna, L. Genesis, Challenges and Opportunities for Colloidal Lead Halide Perovskite Nanocrystals. *Nat. Mater.* **2018**, *17*, 394–405.
- (2) Chun, F.; Zhang, B.; Li, Y.; Li, W.; Xie, M.; Peng, X.; Yan, C.; Chen, Z.; Zhang, H.; Yang, W. Internally-externally Defects-Tailored MAPbI_3 Perovskites with Highly Enhanced Air Stability and Quantum Yield. *Chem. Eng. J.* **2020**, *399*, No. 125715.
- (3) Xie, M.; Liu, H.; Chun, F.; Deng, W.; Luo, C.; Zhu, Z.; Yang, M.; Li, Y.; Li, W.; Yan, W.; et al. Aqueous Phase Exfoliating Quasi-2D CsPbBr_3 Nanosheets with Ultrahigh Intrinsic Water Stability. *Small* **2019**, *15*, No. 1901994.
- (4) Gao, Y.; Luo, C.; Yan, C.; Li, W.; Liu, C.; Yang, W. Copper-Doping Defect-Lowered Perovskite Nanosheets for Deep-Blue Light-Emitting Diodes. *J. Colloid Interface Sci.* **2022**, *607*, 1796–1804.
- (5) Luo, C.; Zhao, Y.; Wang, X.; Gao, F.; Zhao, Q. Self-Induced Type-I Band Alignment at Surface Grain Boundaries for Highly Efficient and Stable Perovskite Solar Cells. *Adv. Mater.* **2021**, *33*, No. 2103231.
- (6) Zeng, X.; Li, W.; Yan, C.; Cao, J.; Fu, X.; Yang, W. Crystallization Control via a Molecular Needle Knitting Strategy for the Enhanced Emission Efficiency and Stability of CsPbBr_3 Films. *J. Mater. Chem. C* **2021**, *9*, 15967–15976.
- (7) Peng, X.; Yan, C.; Chun, F.; Li, W.; Fu, X.; Yang, W. A Review of Low-Dimensional Metal Halide Perovskites for Blue Light Emitting Diodes. *J. Alloys Compd.* **2021**, *883*, No. 160727.
- (8) Kim, Y.-H.; Kim, S.; Kakekhani, A.; Park, J.; Park, J.; Lee, Y.-H.; Xu, H.; Nagane, S.; Wexler, R. B.; Kim, D.-H.; Jo, S. H.; et al. Comprehensive Defect Suppression in Perovskite Nanocrystals for High-Efficiency Light-Emitting Diodes. *Nat. Photonics* **2021**, *15*, 148–155.
- (9) Wang, Y. K.; Yuan, F.; Dong, Y.; Li, J. Y.; Johnston, A.; Chen, B.; Saidaminov, M. I.; Zhou, C.; Zheng, X.; Hou, Y.; et al. All-Inorganic Quantum-Dot LEDs Based on a Phase-Stabilized Alpha-C spbI_3 Perovskite. *Angew. Chem., Int. Ed.* **2021**, *60*, 16164–16170.
- (10) Yao, J.; Wang, L.; Wang, K.; Yin, Y.; Yang, J.; Zhang, Q.; Yao, H. Calcium-Tributylphosphine Oxide Passivation Enables the Efficiency of Pure-Blue Perovskite Light-Emitting Diode up to 3.3%. *Sci. Bull.* **2020**, *65*, 1150–1153.
- (11) Bi, C.; Yao, Z.; Sun, X.; Wei, X.; Wang, J.; Tian, J. Perovskite Quantum Dots with Ultralow Trap Density by Acid Etching-Driven Ligand Exchange for High Luminance and Stable Pure-Blue Light-Emitting Diodes. *Adv. Mater.* **2021**, *33*, No. 2006722.
- (12) Luo, C.; Yan, C.; Li, W.; Chun, F.; Xie, M.; Zhu, Z.; Gao, Y.; Guo, B.; Yang, W. Ultrafast Thermodynamic Control for Stable and Efficient Mixed Halide Perovskite Nanocrystals. *Adv. Funct. Mater.* **2020**, *30*, No. 2000026.
- (13) Zou, G.; Chen, Z.; Li, Z.; Yip, H.-L. Blue Perovskite Light-emitting Diodes: Opportunities and Challenges. *Acta Phys. -Chim. Sin.* **2020**, *37*, No. 2009002.
- (14) Li, Z.; Chen, Z.; Yang, Y.; Xue, Q.; Yip, H. L.; Cao, Y. Modulation of Recombination Zone Position for Quasi-Two-Dimensional Blue Perovskite Light-Emitting Diodes with Efficiency Exceeding 5%. *Nat. Commun.* **2019**, *10*, No. 1027.
- (15) Dong, Y.; Wang, Y. K.; Yuan, F.; Johnston, A.; Liu, Y.; Ma, D.; Choi, M. J.; Chen, B.; Chekini, M.; Baek, S. W.; et al. Bipolar-Shell Resurfacing for Blue LEDs Based on Strongly Confined Perovskite Quantum Dots. *Nat. Nanotechnol.* **2020**, *15*, 668–674.
- (16) Luo, C.; Li, W.; Xiong, D.; Fu, J.; Yang, W. Surface Pre-Optimization of a Mixed Halide Perovskite Toward High Photoluminescence Quantum Yield in the Blue Spectrum Range. *Nanoscale* **2019**, *11*, 15206–15215.
- (17) Li, G.; Rivarola, F. W.; Davis, N. J.; Bai, S.; Jellicoe, T. C.; De la Pena, F.; Hou, S.; Ducati, C.; Gao, F.; Friend, R. H.; et al. Highly Efficient Perovskite Nanocrystal Light-Emitting Diodes Enabled by a Universal Crosslinking Method. *Adv. Mater.* **2016**, *28*, 3528–3534.
- (18) Peng, S.; Wang, S.; Zhao, D.; Li, X.; Liang, C.; Xia, J.; Zhang, T.; Xing, G.; Tang, Z. Pure Bromide-Based Perovskite Nanoplatelets for Blue Light-Emitting Diodes. *Small Methods* **2019**, *3*, No. 1900196.
- (19) Wang, S.; Bi, C.; Yuan, J.; Zhang, L.; Tian, J.; et al. Core-Shell Structure of Cubic CsPbBr_3 @Amorphous CsPbBr_x Perovskite Quantum Dots with a High Blue Photoluminescence Quantum Yield of over 80%. *ACS Energy Lett.* **2018**, *3*, 245–251.
- (20) Bohn, B. J.; Tong, Y.; Gramlich, M.; Lai, M. L.; Doblinger, M.; Wang, K.; Hoye, R. L. Z.; Muller-Buschbaum, P.; Stranks, S. D.; Urban, A. S.; Polavarapu, L.; et al. Boosting Tunable Blue Luminescence of Halide Perovskite Nanoplatelets through Postsynthetic Surface Trap Repair. *Nano Lett.* **2018**, *18*, 5231–5238.
- (21) LaMer, V. K.; Dinegar, R. H. Theory, Production and Mechanism of Formation of Monodispersed Hydrosols. *J. Am. Chem. Soc.* **1950**, *72*, 4847–4854.
- (22) Wang, K.; Reeber, R. R. Thermal Defects and Thermal Expansion of Ionic Crystals at High Temperatures. *Phys. Status Solidi A* **1994**, *146*, 621–627.
- (23) Pan, J.; Quan, L. N.; Zhao, Y.; Peng, W.; Murali, B.; Sarmah, S. P.; Yuan, M.; Sinatra, L.; Alyami, N. M.; Liu, J.; et al. Highly Efficient Perovskite-Quantum-Dot Light-Emitting Diodes by Surface Engineering. *Adv. Mater.* **2016**, *28*, 8718–8725.
- (24) Anderson, N. C.; Hendricks, M. P.; Choi, J. J.; Owen, J. S. Ligand Exchange and the Stoichiometry of Metal Chalcogenide Nanocrystals: Spectroscopic Observation of Facile Metal-Carboxylate Displacement and Binding. *J. Am. Chem. Soc.* **2013**, *135*, 18536–18548.
- (25) Zhang, B. B.; Yuan, S.; Ma, J. P.; Zhou, Y.; Hou, J.; Chen, X.; Zheng, W.; Shen, H.; Wang, X. C.; Sun, B.; et al. General Mild Reaction Creates Highly Luminescent Organic-Ligand-Lacking Halide Perovskite Nanocrystals for Efficient Light-Emitting Diodes. *J. Am. Chem. Soc.* **2019**, *141*, 15423–15432.
- (26) Song, J.; Fang, T.; Li, J.; Xu, L.; Zhang, F.; Han, B.; Shan, Q.; Zeng, H. Organic-Inorganic Hybrid Passivation Enables Perovskite QLEDs with an EQE of 16.48%. *Adv. Mater.* **2018**, *30*, No. 1805409.
- (27) Zhang, F.; Zhong, H.; Chen, C.; Wu, X.-g.; Hu, X.; Huang, H.; Han, J.; Zou, B.; Dong, Y. Brightly Luminescent and Color-Tunable Colloidal $\text{CH}_3\text{NH}_3\text{PbX}_3$ (X = Br, I, Cl) Quantum Dots: Potential Alternatives for Display Technology. *ACS Nano* **2015**, *9*, 4533–4542.

- (28) Huang, H.; Raith, J.; Kershaw, S. V.; Kalytchuk, S.; Tomanec, O.; Jing, L.; Susha, A. S.; Zboril, R.; Rogach, A. L. Growth Mechanism of Strongly Emitting $\text{CH}_3\text{NH}_3\text{PbBr}_3$ Perovskite Nanocrystals with a Tunable Bandgap. *Nat. Commun.* **2017**, *8*, No. 996.
- (29) Huang, H.; Susha, A. S.; Kershaw, S. V.; Hung, T. F.; Rogach, A. L. Control of Emission Color of High Quantum Yield $\text{CH}_3\text{NH}_3\text{PbBr}_3$ Perovskite Quantum Dots by Precipitation Temperature. *Adv. Sci.* **2015**, *2*, No. 1500194.
- (30) Kim, Y. H.; Wolf, C.; Kim, Y. T.; Cho, H.; Kwon, W.; Do, S.; Sadhanala, A.; Park, C. G.; Rhee, S. W.; Im, S. H.; et al. Highly Efficient Light-Emitting Diodes of Colloidal Metal-Halide Perovskite Nanocrystals beyond Quantum Size. *ACS Nano* **2017**, *11*, 6586–6593.
- (31) Zhang, F.; Xiao, C.; Li, Y.; Zhang, X.; Tang, J.; Chang, S.; Pei, Q.; Zhong, H. Gram-Scale Synthesis of Blue-Emitting $\text{CH}_3\text{NH}_3\text{PbBr}_3$ Quantum Dots Through Phase Transfer Strategy. *Front. Chem.* **2018**, *6*, No. 444.
- (32) Yang, F.; Chen, H.; Zhang, R.; Liu, X.; Zhang, W.; Zhang, J.; Gao, F.; Wang, L. Efficient and Spectrally Stable Blue Perovskite Light-Emitting Diodes Based on Potassium Passivated Nanocrystals. *Adv. Funct. Mater.* **2020**, *30*, No. 1908760.
- (33) Cao, J.; Yan, C.; Luo, C.; Li, W.; Zeng, X.; Xu, Z.; Fu, X.; Wang, Q.; Chu, X.; Huang, H.; et al. Cryogenic-Temperature Thermodynamically Suppressed and Strongly Confined CsPbBr_3 Quantum Dots for Deeply Blue Light-Emitting Diodes. *Adv. Opt. Mater.* **2021**, *9*, No. 2100300.
- (34) Rana, S.; Awasthi, K.; Bhosale, S. S.; Diao, E. W.-G.; Ohta, N. Temperature-Dependent Electroabsorption and Electrophotoluminescence and Exciton Binding Energy in MAPbBr_3 Perovskite Quantum Dots. *J. Phys. Chem. C* **2019**, *123*, 19927–19937.
- (35) Nordin, M. N.; Li, J.; Clowes, S. K.; Curry, R. J. Temperature Dependent Optical Properties of PbS Nanocrystals. *Nanotechnology* **2012**, *23*, No. 275701.
- (36) Aristidou, N.; Eames, C.; Sanchez-Molina, I.; Bu, X.; Kosco, J.; Islam, M. S.; Haque, S. A. Fast Oxygen Diffusion and Iodide Defects Mediate Oxygen-Induced Degradation of Perovskite Solar Cells. *Nat. Commun.* **2017**, *8*, No. 15218.
- (37) Shynkarenko, Y.; Bodnarchuk, M. I.; Bernasconi, C.; Berezovska, Y.; Verteletskyi, V.; Ochsenbein, S. T.; Kovalenko, M. V. Direct Synthesis of Quaternary Alkylammonium-Capped Perovskite Nanocrystals for Efficient Blue and Green Light-Emitting Diodes. *ACS Energy Lett.* **2019**, *4*, 2703–2711.
- (38) Liu, P.; Chen, W.; Wang, W.; Xu, B.; Wu, D.; Hao, J.; Cao, W.; Fang, F.; Li, Y.; Zeng, Y.; et al. Halide-Rich Synthesized Cesium Lead Bromide Perovskite Nanocrystals for Light-Emitting Diodes with Improved Performance. *Chem. Mater.* **2017**, *29*, 5168–5173.
- (39) Liu, M.; Zhong, G.; Yin, Y.; Miao, J.; Li, K.; Wang, C.; Xu, X.; Shen, C.; Meng, H. Aluminum-Doped Cesium Lead Bromide Perovskite Nanocrystals with Stable Blue Photoluminescence Used for Display Backlight. *Adv. Sci.* **2017**, *4*, No. 1700335.
- (40) Lu, C. H.; Biesold-McGee, G. V.; Liu, Y.; Kang, Z.; Lin, Z. Doping and Ion Substitution in Colloidal Metal Halide Perovskite Nanocrystals. *Chem. Soc. Rev.* **2020**, *49*, 4953–5007.
- (41) Brennan, M. C.; Herr, J. E.; Nguyen-Beck, T. S.; Zinna, J.; Draguta, S.; Rouvimov, S.; Parkhill, J.; Kuno, M. Origin of the Size-Dependent Stokes Shift in CsPbBr_3 Perovskite Nanocrystals. *J. Am. Chem. Soc.* **2017**, *139*, 12201–12208.
- (42) Pan, J.; Fang, F.; Xie, J.; Wang, L.; Chen, J.; Chang, J.; Lei, W.; Zhang, W.; Zhao, D. Synergistic Effects of Charge Transport Engineering and Passivation Enabling Efficient Inverted Perovskite Quantum-Dot Light-Emitting Diodes. *J. Mater. Chem. C* **2020**, *8*, 5572–5579.
- (43) Wu, Y.; Wei, C.; Li, X.; Li, Y.; Qiu, S.; Shen, W.; Cai, B.; Sun, Z.; Yang, D.; Deng, Z.; Zeng, H. In Situ Passivation of PbBr_6^{4-} Octahedra toward Blue Luminescent CsPbBr_3 Nanoplatelets with Near 100% Absolute Quantum Yield. *ACS Energy Lett.* **2018**, *3*, 2030–2037.
- (44) Abdi-Jalebi, M.; Andaji-Garmaroudi, Z.; Cacovich, S.; Stavrakas, C.; Philippe, B.; Richter, J. M.; Alsari, M.; Booker, E. P.; Hutter, E. M.; Pearson, A. J.; et al. Maximizing and Stabilizing Luminescence from Halide Perovskites with Potassium Passivation. *Nature* **2018**, *555*, 497–501.
- (45) Yang, Z.; Wang, M.; Qiu, H.; Yao, X.; Lao, X.; Xu, S.; Lin, Z.; Sun, L.; Shao, J. Engineering the Exciton Dissociation in Quantum-Confined 2D CsPbBr_3 Nanosheet Films. *Adv. Funct. Mater.* **2018**, *28*, No. 1705908.
- (46) Cai, B.; Li, X.; Gu, Y.; Harb, M.; Li, J.; Xie, M.; Cao, F.; Song, J.; Zhang, S.; Cavallo, L.; Zeng, H. Quantum Confinement Effect of Two-Dimensional All-inorganic Halide Perovskites. *Sci. China Mater.* **2017**, *60*, 811–818.
- (47) Yan, C.; Luo, C.; Li, W.; Peng, X.; Cao, J.; Zeng, X.; Gao, Y.; Fu, X.; Chu, X.; Deng, W.; et al. Thermodynamics Induced Injection Enhanced Deep-Blue Perovskite Quantum Dot LEDs. *ACS Appl. Mater. Interfaces* **2021**, *13*, 57560–57566.
- (48) Hu, H.; Wu, L.; Tan, Y.; Zhong, Q.; Chen, M.; Qiu, Y.; Yang, D.; Sun, B.; Zhang, Q.; Yin, Y. Interfacial Synthesis of Highly Stable CsPbX_3 /Oxide Janus Nanoparticles. *J. Am. Chem. Soc.* **2018**, *140*, 406–412.
- (49) Shen, Y.; Shen, K. C.; Li, Y. Q.; Guo, M.; Wang, J.; Ye, Y.; Xie, F. M.; Ren, H.; Gao, X.; Song, F.; et al. Interfacial Potassium-Guided Grain Growth for Efficient Deep-Blue Perovskite Light-Emitting Diodes. *Adv. Funct. Mater.* **2020**, *31*, No. 2006736.



JACS Au
AN OPEN ACCESS JOURNAL OF THE AMERICAN CHEMICAL SOCIETY

Editor-in-Chief
Prof. Christopher W. Jones
Georgia Institute of Technology, USA

Open for Submissions

pubs.acs.org/jacsau

ACS Publications
Most Trusted. Most Cited. Most Read.